Available online at www.sciencedirect.com
ScienceDirect
Scripta Materialia 59 (2008) 332–335
Scripta MATERIALIA
www.elsevier.com/locate/scriptamat

Photocatalytic properties BiOCl and Bi_2O_3 nanofibers prepared by electrospinning

Changhua Wang,[a,b] Changlu Shao,[c] Yichun Liu[c,*] and Lina Zhang[c]

[a]*Key Laboratory of Excited State Processes, Changchun Institute of Optics, Fine Mechanics and Physics, Chinese Academy of Sciences, Changchun 130033, China*
[b]*Graduate University of Chinese Academy of Science, Beijing 100049, China*
[c]*Centre for Advanced Optoelectronic Functional Materials Research, Northeast Normal University, Changchun 130024, China*

Received 10 January 2008; revised 10 March 2008; accepted 29 March 2008
Available online 9 April 2008

A simple electrospinning method was used to fabricate polymer/inorganic composite fibers from solutions containing polyacrylonitrile (PAN) and $BiCl_3$, and PAN and $Bi(NO_3)_3$, respectively. By performing a calcining process for the composite fibers at 500 °C for 10 h, BiOCl and Bi_2O_3 nanofibers were successfully prepared. The as-prepared BiOCl and Bi_2O_3 nanofibers exhibit tetragonal and β phase, respectively. The photocatalytic test shows that BiOCl and Bi_2O_3 nanofibers possess photocatalytic properties with regard to decomposing rhodamine B under ultraviolet light.

Keywords: Electrospinning; Nanofibers; Photocatalyst; PAN

Photocatalysis, a "green" technique, offers the potential for complete elimination of toxic chemicals in the environment through its efficiency and broad applicability [1]. Thus, in recent years, many photocatalysts have been developed for creating a comfortable environment. In general, two strategies can be exploited to develop photocatalysts. One involves modification of TiO_2 [2–4]. The other one is to search for novel semiconductor materials [5–7]. With regard to the latter, Bi(III)-based oxychlorides and oxide compounds have recently attracted particular interest as photocatalysts. Examples of efficient Bi-based photocatalysts include BiOCl and Bi_2O_3 [8,9]. Bulk BiOCl and Bi_2O_3 with large grain sizes, however, have some disadvantages such as small specific surface areas, long migration distances for the photoexcited electron–hole pairs and an increase in the recombination of the electron–hole pairs, which adversely affect the photocatalytic activities. Interestingly, if the grain sizes are reduced from micro-size to nano-size, the catalytic activities can be dramatically increased [10–12]. Hence preparation of nanostructured BiOCl and Bi_2O_3 photocatalysts doubtless deserves to be taken into account in future research. To this end, nanocrystalline Bi_2O_3 has been successfully prepared and it has proved effective, efficiently breaking down methyl orange pollutant in water under visible light [13]. However, the use of bismuth oxide nanoparticles is often limited, because the suspended particulate catalysts are easily lost in the process of photocatalytic reaction and separation, and may repollute treated water. Instead of nanoparticles, nanofibers, which are an important subclass of nonstructural materials, are viewed as potential candidates for practical application due to their high photocatalytic activity and favorable recycling characteristics [14].

Since electrospinning is a straightforward and convenient method to synthesize nanofibers, there has been intense research on the fabrication of inorganic oxide nanofibers by this method [15–17]. Nevertheless, little work has yet been reported on BiOCl and Bi_2O_3 nanofibers. In this work, BiOCl and Bi_2O_3 nanofibers are prepared by electrospinning precursor mixtures of, respectively, PAN + $BiCl_3$ and PAN + $Bi(NO_3)_3$, followed by careful sintering of the electrospun polymer/inorganic composite fibers at 500 °C for 10 h. The as-synthesized nanofibers exhibit catalytic properties, and as long fibers can be reclaimed easily, they may serve as good potential candidates for photocatalytic application.

For the preparation of BiOCl nanofibers, a PAN solution of about 10.0 wt.% was first prepared by dissolving PAN powder in *N*,*N*-dimethyl formamide and stirring for 2 h. $BiCl_3$ (0.2 g) was then added to 20 ml

* Corresponding author. Tel.: +86 431 5099168; fax: +86 431 5684009; e-mail: ycliu@nenu.edu.cn

1359-6462/$ - see front matter © 2008 Acta Materialia Inc. Published by Elsevier Ltd. All rights reserved.
doi:10.1016/j.scriptamat.2008.03.038

of as-prepared PAN solution, followed by vigorous stirring at room temperature for 4 h to form a homogeneous viscous solution. The viscous solution was then drawn into a plastic syringe equipped with a capillary. A copper pin connected to a high-voltage generator was placed in the solution. A piece of flat aluminum foil was placed about 10 cm below the tip of the needle. The applied electric voltage between the collector and the needle tip was 10 kV. Finally, the electrospinning composite nanofibers were calcined at 500 °C at a heating rate of 2 °C min^{-1} and remained for 10 h to obtain BiOCl nanofibers. In the preparation of Bi_2O_3 nanofibers, 1.0 g of $Bi(NO_3)_3$ was added to 20 ml of 10.0 wt.% PAN solution; other preparation conditions were identical to those of the BiOCl nanofibers.

Fourier transform infrared (FT-IR) spectra were obtained on a Magna 560 FT-IR spectrometer. UV–Vis diffuse reflectance (DR) spectra of the samples were recorded on a Cary 500 UV–Vis–NIR spectrophotometer. X-ray diffraction (XRD) patterns of the samples were recorded on a Rigaku D/max-2500 X-ray diffractometer. Field emission scanning electron microscopy was performed on a Hitachi S-4800 microscope. X-ray photoelectron spectroscopy (XPS) was performed on a VG-ADES 400 instrument with Mg K_α ADES (hv = 1253.6 eV) source at a residual gas pressure of below 10^{-8} Pa. The spectrometer was calibrated by assuming the binding energy of the Au 4f 7/2 line to be 83.9 eV with respect to the Fermi level. As an internal reference for the peak positions, the C1s peak of the surface adventitious carbon has been assumed to be 284.8 eV.

The photoreactor was designed with an internal light source (50 W high-pressure mercury lamp with a main emission wavelength of 313 nm) surrounded by a quartz jacket, where the suspension includes the nanofiber catalyst and an aqueous rhodamine B (RB) solution (100 ml, 20 mg l^{-1}) completely surrounding the light source. The suspension was stirred in the dark for 30 min to obtain a good dispersion and establish adsorption–desorption equilibrium between the organic molecules and the catalyst surface. Decreases in the concentrations of dyes were analyzed by a Cary 500 UV–Vis–NIR spectrophotometer at $\lambda = 554$ nm. At given intervals of illumination, the samples of the reaction solution were taken out, and then centrifuged and filtrated. Finally, the filtrates were analyzed.

Figure 1 shows the XRD patterns of BiOCl and Bi_2O_3 nanofibers. For BiOCl (Fig. 1A), all the peaks can be well indexed to the tetragonal phase (space group: *P*4/*nmm* (129), Joint Committee on Powder Diffraction Standards (JCPDS) File No. 85-861). The strong and sharp diffraction peaks indicate a high degree of crystallization. The calculated lattice constants ($a = b = 0.3890$ nm, $c = 0.7369$ nm) for BiOCl are consistent with the known lattice constants for crystalline BiOCl ($a = b = 0.3883$ nm, $c = 0.7370$ nm). In the pattern of Bi_2O_3 nanofibers (Fig. 1B), very few, if any, impurity peaks are presented. The pattern matches well with the β phase of Bi_2O_3 (space group: *P*-421*c* (114), JCPDS File No. 78-1793). The calculated lattice constants are $a = b = 0.7744$ nm and $c = 0.5638$ nm, which are consistent with the reported data ($a = b = 0.7741$ nm and $c = 0.5634$ nm).

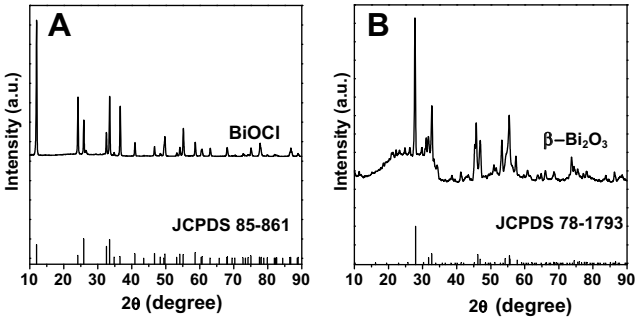

Figure 1. (A) XRD pattern of BiOCl nanofibers and the standard pattern of tetragonal BiOCl; (B) XRD pattern of Bi_2O_3 nanofibers and the standard pattern of β-Bi_2O_3.

FT-IR spectra were employed to confirm the removal of the polymer, and the results are shown in Figure 2. Figure 2B shows the IR spectra of as-prepared BiOCl nanofibers. It can be clearly seen that the characteristic peaks of the PAN have disappeared (compared with Fig. 2A) after heating at 500 °C for 10 h, which indicates that the polymer has been degraded completely at this temperature. In addition, a band corresponding to valent symmetrical A_{2u}-type vibrations of the Bi–O bond (515 cm^{-1}) in BiOCl [18] is observed, indicating that the BiOCl nanofibers are obtained. Figure 2D shows IR spectra of as-prepared Bi_2O_3 nanofibers. The peaks of the PAN have disappeared (compared with Fig. 2C) and a peak centered at 520 cm^{-1} attributed to vibration of the Bi–O bonds of BiO_6 octahedra in Bi_2O_3 [19] appears, indicating that the organic molecules could be removed completely from PAN/$Bi(NO_3)_3$ composite fibers and that Bi_2O_3 nanofibers have been obtained.

XPS survey scan of the as-prepared nanofibers revealed the presence of Bi, O, Cl and C in BiOCl, and Bi, O and C in Bi_2O_3, respectively. The C1s peak in both BiOCl and Bi_2O_3 at 284.8 eV (see Supplementary material) is derived from a surface layer of contamination carbon. Furthermore, the C1s peak at 286.5 eV for the species associated with groups of PAN [22] is not detected, implying that the organic species are removed completely. Figure 3 shows the XPS spectra of the Bi 4f and Cl 2p. In the case of BiOCl nanofibers, on the one hand, the Bi4f spectra can be deconvoluted into four peaks. The peaks with binding energy of 159.7 and

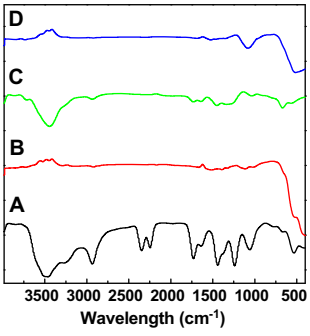

Figure 2. FT-IR spectra of (A) as-spun PAN/$BiCl_3$ nanofibers; (B) BiOCl nanofibers; (C) as-spun PAN/$Bi(NO_3)_3$ nanofibers; (D) Bi_2O_3 nanofibers.

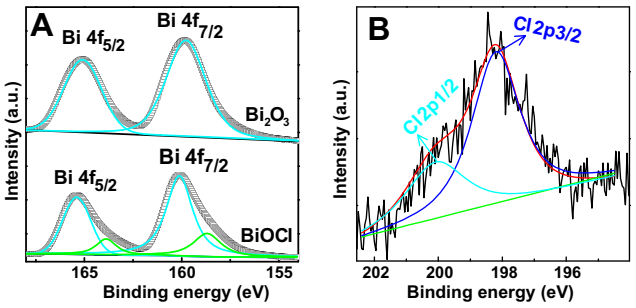

Figure 3. (A) High-resolution XPS survey spectra of Bi 4f in BiOCl and Bi_2O_3 nanofibers; (B) high-resolution XPS survey spectra of Cl 2p in BiOCl nanofibers.

164.9 eV, as displayed in Figure 3A, are for the Bi 4f 7/2 and Bi 4f 5/2 region for BiOCl [20], respectively. The peaks at 158.6 and 163.8 eV should be assigned to Bi 4f 7/2 and Bi 4f 5/2 region from a trace amount of bismuth oxide species [23], respectively, which were possibly formed during the calcination process of PAN/$BiCl_3$ precursor in air. On the other hand, the Cl 2p peak, shown in Figure 3B, is deconvoluted into two peaks (198.2, 200.2 eV), which are assigned, respectively, to the Cl 2p 3/2 and Cl 2p 1/2 region for BiOCl, further confirming that BiOCl nanofibers are formed. In the case of Bi_2O_3 nanofibers, the binding energy peaks located at 159.8 and 165.0 eV are for the Bi 4f 7/2 and Bi 4f 5/2 region for Bi_2O_3 [21], respectively. In addition, the XPS peak positions of Bi 4f demonstrate that the main chemical states of Bi in the two samples are both +3 valence [20,21].

Figure 4 shows SEM images of the as-prepared samples. From Figure 4A, it can be observed that these randomly oriented fibers have a smooth and uniform surface due to the amorphous nature of the PAN/$BiCl_3$ composite nanofibers. Their lengths can reach several micrometers and their diameters range from 250 to 300 nm. The BiOCl nanofibers, the diameters of which range from 80 to 140 nm (Fig. 4B), exhibit shrinkage resulting from the decomposition of PAN. Likewise, the diameters of as-spun PAN/$Bi(NO_3)_3$ nanofibers range from 200 to 300 nm (Fig. 4C) and the diameters of Bi_2O_3 nanofibers range from 70 to 100 nm (Fig. 4D).

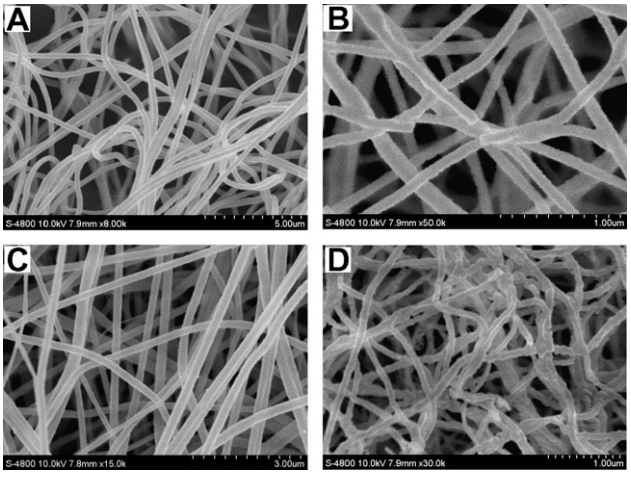

Figure 4. SEM images of (A) as-spun PAN/$BiCl_3$ nanofibers; (B) BiOCl nanofibers; (C) as-spun PAN/$Bi(NO_3)_3$ nanofibers; (D) Bi_2O_3 nanofibers.

Figure 5 shows the UV–Vis DR spectra of BiOCl and Bi_2O_3 nanofibers. The as-prepared BiOCl nanofibers display a white color, the onset of BiOCl is determined at 306 nm and the absorption edge occurs at about 390 nm (Fig. 5A). The band gap energy of the as-prepared BiOCl nanofibers is also determined from a plot of $(\alpha h\nu)^2$ vs. energy ($h\nu$) (Fig. 5B) and is found to be about 3.2 eV. In contrast, the as-prepared Bi_2O_3 nanofibers display a yellow color, the onset of Bi_2O_3 is determined at 256 nm and the absorption edge occurs at about 480 nm. The band gap energy is determined to be about 2.6 eV. As also shown in Figure 5, intense absorption bands with a steep edge for both nanofibers are observed, indicating that the absorption band is induced by the intrinsic band gap transition instead of the transition from impurity levels.

The photocatalytic activities of BiOCl and Bi_2O_3 nanofibers were evaluated. RB was utilized as a model compound for the photocatalytic decomposition of pollutant. The photocatalytic decomposition is plotted as irradiation time vs. $\ln C_0/C$, and showed approximately first-order kinetics. That is, the photocatalytic reaction can simply be described by $-\mathrm{d}[c]/\mathrm{d}t = kr[c]$, where [c] is the concentration of RB, t is the irradiation time, and kr is the overall rate constant. Herein, the photocatalytic activity is defined as kr . In this work, the degradation of RB under UV irradiation was not significant in the absence of photocatalyst and no degradation occurred in the presence of the photocatalyst without UV

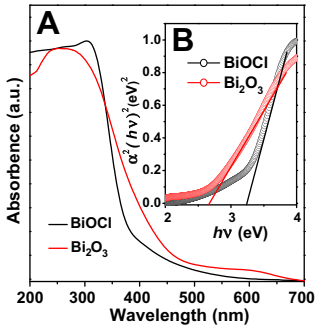

Figure 5. (A) UV–Vis DR spectra of BiOCl and Bi_2O_3 nanofibers; (B) plots of $(\alpha h\nu)^2$ vs. energy ($h\nu$) for the band gap energies.

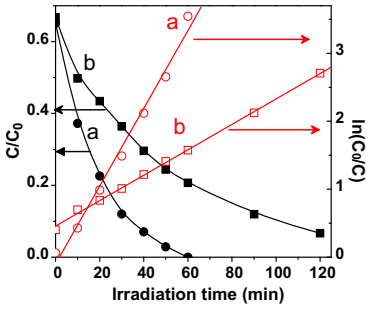

Figure 6. Photocatalytic degradation of RB and kinetic linear simulation curve over (a) BiOCl and (b) Bi_2O_3 nanofibers. $C_0 = 20\ \mathrm{mg\ l^{-1}}$, catalyst 0.08 g.

irradiation (not shown). Figure 6 shows the degradation profiles of RB over BiOCl and Bi_2O_3 nanofibers. It can be observed that RB could be degraded almost completely in the presence of BiOCl nanofibers for 60 min and in the presence of Bi_2O_3 nanofibers for 120 min under UV, respectively. The determined *kr* for BiOCl and Bi_2O_3 nanaofibers are 0.057 and 0.018, respectively. In other words, the photoactivity of BiOCl is three times greater than that of Bi_2O_3.

Many factors, including grain size, morphology, crystallinity and preparation conditions, affect the photoactivity of a photocatalyst. The difference in photocatalytic activity between BiOCl and Bi_2O_3 nanofibers may be attributed to the following factors: (a) the high crystallinity of BiOCl means few defects, which may serve as recombination centers for photoexcited electron–hole pairs during photocatalysis, decreasing the photocatalytic activity; (b) the conduction band minimum is mainly composed of Bi 6p orbitals, whereas the valence band maximum primarily consists of Cl 3p, O 2p and Bi 6p orbitals. The existence of hybrid states leading to good dispersions in the conduction and valence bands in BiOCl can confer good mobility on photogenerated charges, enabling these to travel a long distance, and hence assisting the photostimulated electron–hole separations and improving the photocatalytic activity of BiOCl [8,24].

In addition, given that the feasibility of separating catalyst from solution after reaction is of crucial importance, the sedimentation abilities of the BiOCl and Bi_2O_3 nanofibers were also tested. In this experiment, both the nanofiber catalysts with lengths of the order of micrometers sedimented from an aqueous suspension after a photocatalytic reaction in less than 1 h. The fact that these nanofiber photocatalysts can be easily recovered by sedimentation will greatly promote their industrial application to eliminate organic pollutants from wastewater.

In summary, BiOCl nanofibers with diameters of 80–140 nm and Bi_2O_3 nanofibers with diameters of 70–100 nm were fabricated by using electrospun nanofibers of, respectively, PAN/$BiCl_3$ and PAN/$Bi(NO_3)_3$ as precursors, followed by calcination. XRD, FT-IR, XPS, SEM and UV–Vis results suggested the formation of BiOCl and β-Bi_2O_3 nanofibers. The as-prepared nanofibers possess photocatalytic activity and sedimentation ability. This method also provides a simple and versatile way to prepare other active photocatalysts for industrial application.

This work is supported by National High Technology Research and Development Program of China (2006AA03Z311), the Cultivation Fund of the Key Scientific and Technical Innovation Project (Grant No. 704017), the Ministry of Education of China, National Natural Science Foundation of China (Grant No. 60576040 and 50572014).

Supplementary data associated with this article can be found, in the online version, at doi:10.1016/j.scriptamat. 2008.03.038.

[1] M.R. Hoffmann, S.T. Martin, W. Choi, D.W. Bahnemann, Chem. Rev. 95 (1995) 69.
[2] R. Asahi, T. Morikawa, T. Ohwaki, K. Aoki, Y. Taga, Science 293 (2001) 269.
[3] X.T. Hong, Z.P. Wang, W.M. Cai, F. Lu, J. Zhang, Y.Z. Yang, N. Ma, Y.J. Liu, Chem. Mater. 17 (2005) 1548.
[4] S. Sakthivel, H. Kisch, Angew. Chem. Int. Ed. 42 (2003) 4908.
[5] K. Maeda, T. Takata, M. Hara, N. Saito, Y. Inoue, H. Kobayashi, K. Domen, J. Am. Chem. Soc. 127 (2005) 8286.
[6] H. Hagiwara, N. Ono, T. Inoue, H. Matsumoto, T. Ishihara, Angew. Chem. Int. Ed. 45 (2006) 1420.
[7] F. Gao, X.Y. Chen, K.B. Yin, S. Dong, Z.F. Ren, F. Yuan, T. Yu, Z.G. Zou, J.M. Liu, Adv. Mater. 19 (2007) 2889.
[8] K.L. Zhang, C.M. Liu, F.Q. Huang, C. Zheng, W.D. Wang, Appl. Catal. B 68 (2006) 125.
[9] Y. Bessekhouad, D. Robert, J.V. Weber, Catal. Today 101 (2005) 315.
[10] L. Zhang, J. Lin, Z. Chen, Y. Tang, Y. Yu, Appl. Catal. A: Gen. 299 (2006) 292.
[11] J.C. Yu, J.G. Yu, W.K. Ho, L.Z. Zhang, Chem. Commun. (2001) 1942.
[12] T. Park, S.A. Haque, R.J. Potter, A.B. Holmes, J.R. Durrant, Chem. Commun. (2003) 2878.
[13] L.S. Zhang, W.Z. Wang, J. Yang, Z.G. Chen, W.Q. Zhang, L. Zhou, S.W. Liu, Appl. Catal. A: Gen. 308 (2006) 105.
[14] Z.Y. Liu, D.D. Sun, P. Guo, J.O. Leckie, Nano Lett. 7 (2007) 1081.
[15] H.Y. Guan, C.L. Shao, B. Chen, J. Gong, X.H. Yang, Inorg. Chem. Commun. 6 (2003) 1409.
[16] C.L. Shao, H.Y. Guan, Y.C. Liu, X.L. Li, X.H. Yang, J. Solid State Chem. 177 (2004) 2628.
[17] D. Li, Y.N. Xia, Adv. Mater. 16 (2004) 1151.
[18] M.N. Novokreshchenova, Yu. Yukhin, B.B. Bokhonov, Chem. Sustain. Develop. 13 (2005) 563.
[19] F. Miyaji, T. Yoko, S. Sakka, J. Non-Cryst. Solids 126 (1990) 170.
[20] W.E. Morgan, W.J. Stec, J.R. Vanwazer, Inorg. Chem. 12 (1973) 953.
[21] V.S. Dharmadhikari, S.R. Sainkar, S. Badrinarayan, A. Goswami, J. Electron Spectrosc. Relat. Phenom. 25 (1982) 181.
[22] High Resolution XPS of Organic Polymers: the Scienta ESCA300 Database, 1992.
[23] Y. Schuhl, H. Baussart, R. Delobel, M. Le Bras, J. Leroy, L.G. Gengembre, J. Rimblot, J. Chem. Soc. Faraday Trans. 79 (1983) 2055.
[24] W.D. Wang, F.Q. Huang, X.P. Lin, Scripta Mater. 56 (2007) 669.